Journal of Materials Chemistry A

Accepted Manuscript

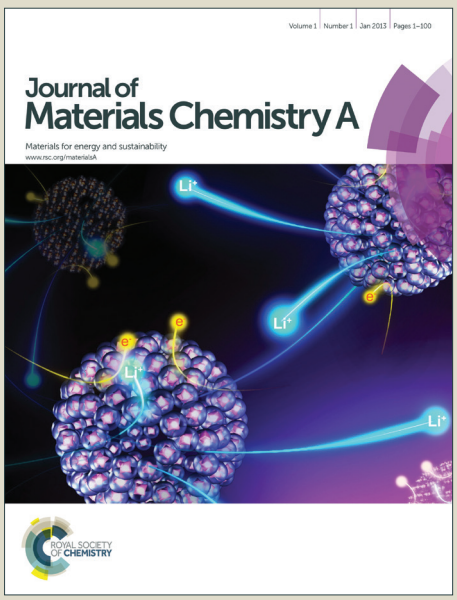

ROYAL SOCIETY OF CHEMISTRY

www.rsc.org/materialsA

Controllable synthesis of high-performance $LiMnPO_4$ nanocrystals by a facile one-pot solvothermal process

Hui Guo,[a] Chunyang Wu,[b] Jian Xie,[ab] Shichao Zhang,[c] Gaoshao Cao*[ab] and Xinbing Zhao[ab]

[a]*State Key Laboratory of Silicon Materials, Department of Materials Science and Engineering, Zhejiang University, Hangzhou 310027, China. E-mail: xiejian1977@zju.edu.cn; Fax: +86-571-87951451; Tel: +86-571-87952181*
[b]*Key Laboratory of Advanced Materials and Applications for Batteries of Zhejiang Province, China*
[c]*School of Materials Science and Engineering, Beijing University of Aeronautics and Astronautics, Beijing 100191, China*

Abstract

Olivine-type $LiMnPO_4$ has been considering as a promising cathode for next-generation high-power lithium ion batteries. Preparing high-performance $LiMnPO_4$ cathode by a simple approach has been a subject of much scientific inquiry for many years. We report here a simple solvothermal synthesis of $LiMnPO_4$ nanocrystals using $LiOH{\cdot}H_2O$, H_3PO_4 and $MnSO_4{\cdot}H_2O$ as precursor and ethylene glycol as reaction medium. We found that the ratio of the starting materials exerts a great influence on the morphology, size and crystal orientation of $LiMnPO_4$ nanocrystals. We confirmed the critical role that H^+ concentration plays in altering the crystallization habit of $LiMnPO_4$. The results showed that after carbon coating, the plate-like $LiMnPO_4$, which was synthesized from the precursor with a $LiOH/H_3PO_4/MnSO_4$ ratio of 3:1.1:1, exhibited the best electrochemical performance, yielding a discharge capacity of 108.2 mAh g^{-1} at 10 C and keeping a discharge capacity of 133.5 mAh g^{-1} after 100 cycles at 0.5 C. This simple, one-spot solvothermal preparation method sheds light on the synthesis of high-performance $LiMnPO_4$ cathode material.

Introduction

Olivine-structure $LiMPO_4$ (M = Fe, Mn) as hosts for lithium ions has attracted a great attention as new cathode materials since they were first reported in 1997 by Goodenough and co-workers.[1] Their environmental benignancy, low cost and excellent thermal stability make them very promising candidates of cathode materials that used in the high-power systems such as hybrid electric vehicles (HEVs) and electric vehicles (EVs).[2-5] Compared to $LiFePO_4$, $LiMnPO_4$ offers a larger energy density due to its higher Mn^{2+}/Mn^{3+} redox potential (4.1 V vs. Li/Li^+) than the Fe^{2+}/Fe^{3+} (3.45 V vs. Li/Li^+) and it has become the focus of interest to replace commercialized $LiFePO_4/C$ as next-generation cathode.[3, 5, 6] However, except for the intrinsically lower electronic and ionic conductivities than $LiFePO_4$, $LiMnPO_4$ also suffers from Jahn-Teller lattice distortion in Mn^{3+} sites and the interface strain between $LiMnPO_4$ and $MnPO_4$.[5] All these disadvantages lead to

unsatisfactory electrochemical performance of $LiMnPO_4$ such as low capacity, poor rate performance and short cycle life.

Tremendous effort has been made in recent years to overcome these limitations. Among various strategies, carbon coating and particle size reduction seem to be the most effective way considering the sluggish electron and ion transport in $LiMnPO_4$ framework. The electrochemical performance of $LiMnPO_4$ has been significantly improved by using these strategies.[6-9] In 2009, Martha *et al.*[7] prepared platelet-like $LiMnPO_4$ composed of 25–30 nm particles. This material could deliver practical capacities of 140 mAh g^{-1} and 120 mAh g^{-1} at 0.1 C and 0.5 C, respectively, after being coated with 15 nm thick carbon layer, In 2010, Oh *et al.*[6] synthesized a carbon-$LiMnPO_4$ nanocomposite by ultrasonic spray pyrolysis followed by ball milling with 30 wt% acetylene black. The composite could deliver discharge capacities of 158 mAh g^{-1} at C/20, 126 mAh g^{-1} at 1 C, and 107 mAh g^{-1} at 2 C. Later, Rui *et al.*[9] designed the ultrathin $LiMnPO_4$ nanosheets (thickness: 3.7 nm) with exposed (010) facets using a liquid-phase exfoliation approach combined with solvothermal lithiation. The carbon-coated $LiMnPO_4$ nanosheets could yield capacities of 119 mAh g^{-1} at 5 C and 95 mAh g^{-1} at 10 C.

However, most of the synthesis of high-performance $LiMnPO_4$ involved a complex process, which limits its large-scale production. Simplifying the synthesis has been a hot subject of scientific research currently. Hydrothermal/solvothermal preparation is one of the facile ways and energy saving methods to prepare nano-sized materials.[10] Due to the simple technique, short reaction time and mild reaction temperature, the soft-chemical preparation has been extensively studied and widely used in various fields.[10-14] Hydrothermal preparation of $LiMPO_4$ was first realized by Yang *et al.* in 2001.[15] To date, several groups have reported the hydrothermal/solvothermal synthesis of

$LiMnPO_4$ and much excellent work has been done in development of this preparation.[16-24] However, a challenge still remains to prepare high-performance $LiMnPO_4$ nanoparticles by hydrothermal/solvothermal route although the particle size was successfully decreased to ~100 nm. Therefore, effective strategies should be conducted to improve this method. Nan *et al*.[25, 26] found that different ratios of starting materials had a significant influence on the particle morphology and crystal orientation. Especially, when the ratio of $LiOH/H_3PO_4$ was set as 2.7:1 (not 3:1 as commonly used), (010) face orientated $LiFePO_4$ nanoplates were obtained and the electrochemical performance has been increased to a large extent. In addition, many researchers have confirmed independently that ethylene glycol (EG), as the reaction medium and mineralizer, plays an important role in reducing the intrinsic defect concentration and enhancing the electrochemical performance of the products.[27-29]

Keeping this in mind, we present here a solvothermal synthesis of $LiMnPO_4$ using LiOH, H_3PO_4 and $MnSO_4$ as the starting materials and EG as the solvent. We first adopted two different ratios of starting materials and compared the electrochemical properties of the products. In one experiment, the $LiOH/H_3PO_4/MnSO_4$ ratio is set at 3:1:1 as commonly used, and the product is named LMP-CR. In the other experiment, $LiOH/H_3PO_4/MnSO_4$ is 2.7:1:1, and the product is named LMP-NR. We observed apparent changes in particle size, morphology and crystal orientation by decreasing the amount of LiOH. We tentatively attributed these changes to the difference in H^+ concentration between the two precursors for $LiMnPO_4$. Accordingly, another two experiments were designed to confirm this assumption, where the ratios of the starting materials are set at $LiOH/H_3PO_4/MnSO_4$=3:1.1:1 (the product name: LMP-VR) and $LiOH/H_3PO_4/MnSO_4/H_2SO_4$=3:1:1:0.15 (the product name: LMP-SR). The electrochemical

measurements of the carbon-coated $LiMnPO_4$ revealed the particle size plays a critical role in determining the electrochemical performance of $LiMnPO_4$. Among the four samples, carbon-coated LMP-VR exhibits the best rate performance, delivering capacities 163.2 mAh g^{-1} at C/20，143.8 mAh g^{-1} at 1 C, 122.5 mAh g^{-1} at 5 C and 108.2 mAh g^{-1} at 10 C. This sample also shows excellent cycling stability with a discharge capacity of 133.5 mAh g^{-1} remained after 100 cycles at 0.5 C.

Experimental section

Solvothermal Synthesis of $LiMnPO_4$ nanoparticles

Preparation of LMP-CR sample: First, solutions of LiOH in EG and H_3PO_4 in EG were prepared separately by adding 0.03 mol $LiOH·H_2O$ and 0.01 mol H_3PO_4 in 40 and 20 ml EG. Meanwhile, 0.01 mol $MnSO_4·H_2O$ was dissolved in 5 ml deionized (DI) water followed by adding 35 ml EG with stirring to form $MnSO_4$ solution. Then, the H_3PO_4 solution was added to the LiOH solution very slowly (less than 1 mL min^{-1}) with vigorous stirring. A white suspension was formed after this mixing process. Afterwards, the $MnSO_4$ solution was introduced slowly to the above white suspension. The final mixture was magnetically stirred for 10 min before it was transferred to a 120 mL Teflon-lined stainless steel autoclave. The solvothermal process was carried out at 180 °C for 10 h. The white precipitate was collected by centrifugation, washed by DI water and absolute ethanol repeatedly and dried at 60 °C for 12 h.

Preparation of LMP-NR sample: the amount of LiOH was decreased to 0.027 mol with other conditions same as LMP-CR ($LiOH/H_3PO_4/MnSO_4$=2.7:1:1).

Preparation of the LMP-VR sample: the amount of H_3PO_4 was increased to 0.011 mol with other conditions same as LMP-CR ($LiOH/H_3PO_4/MnSO_4$=3:1.1:1).

Preparation of LMP-SR sample: 0.015 ml H_2SO_4 aqueous solution (1 mol L^{-1}) was added to the H_3PO_4/EG solution before it was introduced to the LiOH/EG solution, while the other conditions are same as LMP-CR ($LiOH/H_3PO_4/MnSO_4/H_2SO_4$=3:1:1:0.015).

Synthesis of $LiMnPO_4$/C composites

For carbon coating, the solvothermal products were mixed with glucose (the weight ratio of $LiMnPO_4$/glucose is 2:1) in DI water to form dispersions. After drying, the mixture was fired under Ar atmosphere at 600 °C for 4 h with a heating rate of 5 °C min^{-1}. For simplicity, the name of the carbon-coated $LiMnPO_4$ ($LiMnPO_4$/C) is same as that of the corresponding solvothermal product.

Materials Characterization

The crystal structures of the solvothermal products were checked by X-ray diffraction (XRD) on a Rigaku D/Max-2550pc powder diffractometer equipped with Cu K_α radiation radiation (λ = 1.541 Å). The scanning electron microscopy (SEM) images were characterized with an S-4800 field emission scanning electron microscope (Hitachi, Japan). Transmission electron microscopy (TEM) and high-resolution TEM (HRTEM) images were observed with a FEI Tecnai G2 F20 S-Twin high-resolution transmission electron microscope with an acceleration voltage of 200 kV. N_2 absorption/desorption isotherms were collected using a Quantachrome Autosorb-1 analyser. The carbon content analysis of $LiMnPO_4$/C was conducted on a Flash EA 1112 tester.

Electrochemical measurements

The electrochemical performance of $LiMnPO_4$/C was evaluated by galvanostatic cycling using CR2025-type coin cells. The electrode slurry was made by dispersing 70 wt% $LiMnPO_4$/C, 20 wt% acetylene black and 10 wt% polyvinylidene fluoride (PVDF) in N-methyl pyrrolidone (NMP) with magnetic stirring for 2 h. The slurry was then coated uniformly on Al foil and dried at 100 °C under vacuum overnight to make the working electrodes. The active material loading was ~ 2.3 mg cm^{-2}.The electrodes were then assembled into half cells in an Ar-filled glove box using Li foil as the counter electrode and Celgard 2300 membrane as the separator. The electrolyte used was 1 M $LiPF_6$ in ethylene carbonate (EC)/dimethyl carbonate (DMC) (1:1 in volume). The cells were tested in a voltage range of 2.0–4.5 V (vs. Li/Li^+) using a constant-current–constant-voltage (CC–CV) protocol

on a Neware BTS-5V-10mA battery cycler (Shenzhen, China). The cells were charged to 4.5 V at various rates, kept at 4.5 V for 1 h and discharged to 2.0 V at the same rate. The current was set based on the weight of $LiMnPO_4$ and 1 C is 170 mA g^{-1}. The specific capacity was calculated based on the weight of bare $LiMnPO_4$ (excluding ex situ coated carbon). Cyclic voltammetry (CV) scanning was performed on an Arbin BT2000 system in the voltage range 2.0–4.5 V (vs. Li/Li^+) at various scan rates. Electrochemical impedance spectroscopy (EIS) measurements were conducted on a CHI660C electrochemistry workstation by applying an ac voltage of 5 mV amplitude in the frequency range from 10 mHz to 100 kHz. All of the electrochemical measurements were carried out at room temperature.

Results and discussion

Fig. 1 shows the XRD patterns of the solvothermal products synthesized from two different ratios of the starting materials. All the diffraction peaks of LMP-CR and LMP-NR could be indexed to olivine-type $LiMnPO_4$ with a *Pnmb* space group of the orthorhombic system (JCPDS card no. 74–0375) and no impurity phase is detected. It is worth noting that the relative intensity of the diffraction peaks in LMP-NR is quite different from that in LMP-CR. For hydrothermally/solvothermally synthesized $LiFePO_4$ and $LiMnPO_4$, it has been demonstrated that the peak intensity ratio has a strong relationship with the crystal morphology.[25, 29, 30] Thus, the large difference in relative peak intensity between LMP-CR and LMP-NR indicates the different crystal orientation and this will be discussed below.

Fig. 2 gives the SEM images of $LiMnPO_4$ obtained from two different ratios of starting materials. SEM image in Fig.2a indicates that LMP-CR consists of uniform spindle-like crystals and these nano-spindles have a length of ~320 nm, a width of ~120 nm, and a mean thickness of around 50 nm. When a new precursor ratio was adopted, however, the spindle-like shape is transformed to cubic-like thin plates with length and width of 80–130 nm, as shown in Fig. 2b. As

expected, the ratio of the starting materials indeed plays an important role in directing crystal growth during the solvothermal process, leading to a sharp difference in the morphology of $LiMnPO_4$. In addition, this result also indicates size reduction of $LiMnPO_4$ can be realized by simply decreasing the concentration of LiOH, which provides a new method to the preparation of $LiMnPO_4$ nanoparticles.

Fig. 3 shows the TEM and HRTEM images of LMP-CR and LMP-NR, as well as the schematic diagrams and fast fourier transform (FFT) patterns of the two $LiMnPO_4$ samples. In Fig. 3a, the interplanar spacings of 10.47 and 4.74 Å correspond to (100) and (001) lattice planes of $LMnPO_4$, demonstrating that the largest exposed faces of the nano-spindles are (010) planes. At a new ratio of $LiOH/H_3PO_4/MnSO_4$=2.7:1:1, however, the thickness of the $LiMnPO_4$ nanoplates is decreased to less than 20 nm and the obatined nanoplates are mainly expose (001) faces, as identified by HRTEM and FFT in Fig. 3b. The above results suggest that the different ratios in the starting materials have a great influence on both morphology and crystal orientation of $LiMnPO_4$.

The interesting results shown above along with some similar phenomena observed on $LiFePO_4$ raise one question: why and how does the ratio of the starting materials affect the morphology, size and crystal orientation of $LiMnPO_4$? It is wildly accepted that the formation of $LiMnPO_4$ can be expressed by equation (1) when the $LiOH/H_3PO_4/MnSO_4$ ratio is 3:1:1 as commonly used for the hydrothermal/solvothermal synthesis:

$$H_3PO_4 + 3LiOH + MnSO_4 = LiMnPO_4 + Li_2SO_4 + 3H_2O \quad (1)$$

After decreasing the ratio of $LiOH/H_3PO_4$ from 3 to 2.7, we propose the reaction process as equation (2):

$$H_3PO_4 + 2.7LiOH + MnSO_4$$

$$= (0.1H_3PO_4 + 0.1MnSO_4) + 0.9H_3PO_4 + 2.7LiOH + 0.9MnSO_4$$

$= (0.1H_3PO_4 + 0.1MnSO_4) + 0.9LiMnPO_4 + 0.9Li_2SO_4 + 2.7H_2O$ (2)

According to equations (1) and (2), the "relative" proportion of the H_3PO_4 and $MnSO_4$ in the precursor of LMP-NR is increased in comparison with that of LMP-CR. We thus speculate that the "increased H_3PO_4" is the principal reason for the morphology and orientation changes of $LiMnPO_4$. To verify this hypothesis, another experiment was conducted with the ratio of $LiOH/H_3PO_4/MnSO_4$ =3:1.1:1 (the product: LMP-VR). The total reaction process is written in equation (3):

$1.1H_3PO_4 + 3LiOH + MnSO_4$

$= 0.1H_3PO_4 + H_3PO_4 + 3LiOH + MnSO_4$

$= 0.1H_3PO_4 + LiMnPO_4 + Li_2SO_4 + 3H_2O$ (3)

SEM, TEM and FFT in Fig 4a confirm that LMP-VR has the same particle morphology, similar particle size and identical crystal orientation to those of LMP-NR. The thickness of LMP-VR plates is similar to that of LMP-NR plates. The XRD patterns of LMP-VR are also in agreement with those of LMP-NR. The results indicate that, in solvothermal preparation of $LiMnPO_4$, the concentration of H_3PO_4 plays an important role in altering the crystal morphology and orientation.

As reported by Qin et al.[31], for solvothermal synthesis of $LiMnPO_4$, evolution from tetraphosphate compounds to PO_4^{3-} gives rise to H^+ at elevated temperature, leading to a rapid drop in pH of the reaction system. The work by Qin *et al*.[19] and Yang *et al*.[20] demonstrated that pH has an important effect on the morphology of products during the hydrothermal/solvothermal process and the influence of H^+ on the crystal growth was also reported in many other inorganic ions.[32-34] Therefore, it is reasonable to consider that the "extra" H_3PO_4 in the precursors for LMP-NR and LMP-VR actually contributes more H^+ during the reaction process, in comparison with that for LMP-CR. However, it is difficult to precisely determine the pH values before and after the reaction because of low amount of water in the reaction system. Accordingly, we performed another experiment to verify the important role of H^+, where 0.015 ml H_2SO_4 aqueous solution (1 mol L^{-1})

was added to the H_3PO_4/EG solution before it was introduced to the LiOH/EG solution, while other conditions are kept same as LMP-CR ($LiOH/H_3PO_4/MnSO_4/H_2SO_4$ was 3:1:1:0.15, the product: LMP-SR). Similar morphology and same crystal orientation are evident (Fig. 4b). The thickness of LMP-SR plates is somewhat higher than that of LMP-NR plates.The result clearly verifies that the change in concentration of H^+ in the reaction system leads to the morphology and crystal orientation changes of $LiMnPO_4$.

The above results reveal the dependence of the morphology and orientation on the ratios of starting materials. It is unclear yet how H^+ affects the crystal growth during the solvothermal process. Note that both LMP-VR and LMP-SR exhibit some differences in morphology with LMP-NR. SEM image in Fig. 4a shows that compared with LMP-NR, LMP-VR exhibits a wider particle size distribution with lots of smaller nanoparticles (less than 20 nm) generated. This is in agreement with the Brunauer-Emmett-Teller (BET) specific surface area measurements. As given in Table 1, LMP-VR has the largest BET area among the four samples. For LMP-SR, the decrease in BET area compared with LMP-NR indicates that it has a larger average particle dimension, which may result from the decrease in viscosity of the solvent due to the introduction of water in solvent by adding H_2SO_4 aqueous solution.

Table 1. BET specific surface area of $LiMnPO_4$.

Sample	LMP-CR	LMP-NR	LMP-VR	LMP-SR
BET ($m^2\ g^{-1}$)	32.2	64.7	72.4	43.6

Considering the low electronic conductivity of $LiMnPO_4$, all of the four samples were coated with carbon before the electrochemical tests. The carbon contents in LMP-CR, LMP-NR, LMP-VR and LMP-SR are 7.9%, 7.1%, 7.0% and 7.4%, respectively. Fig. 5 shows the discharge curves of the carbon-coated $LiMnPO_4$ samples at various rates ranging from C/20 to 10 C. For the rate capability

tests in our experiments, the cells were charged and discharged at the same current rate. All of the samples exhibit a discharge plateau at around 4.15 V (vs. Li/Li^+) at C/20, corresponding to the redox couple of Mn^{3+}/Mn^{2+} of $LiMnPO_4$ and the plateau is on the decrease with the increase in current rate. Note that LMP-CR shows a discharge capacity of only 105.4 mAh g^{-1} at C/20, and it decreases rapidly to 84.5, 60.7, 55, 46.8, 34.8 and 24.9 mAh g^{-1} at 0.1, 0.5, 1, 2, 5 and 10 C, respectively, as shown in Fig. 5a. In contrast, LMP-NR can deliver a much higher capacity at each current rate (Fig. 5b). Of note is that this obvious performance improvement can be realized by simply adjusting the ratio of the starting materials. Among the four samples, LMP-VR demonstrates the best rate performance. At C/20, it can deliver a discharge capacity of 163.2 mAh g^{-1}, close to the theoretical value of $LiMnPO_4$. The discharge capacities of this sample are 143.8 mAh g^{-1} at 1 C, 136.5 mAh g^{-1} at 2 C, 122.5 mAh g^{-1} at 5 C and 108.2 mAh g^{-1} at 10 C (Fig. 5c), indicating excellent rate capability. The results are superior to those prepared also by the hydrothermal/solvothermal method previously.[17, 19, 20, 22, 23] LMP-SR also exhibits improved rate performance than LMP-CR as shown in Fig. 5d. Note that plate-like $LiMnPO_4$ (LMP-NR, LMP-VR and LMP-SR) with crystal orientation along bc facet delivers much higher capacity than spindle-like $LiMnPO_4$ although the later has a preferred orientation (along ac facet). Therefore, the difference in rate performance is attributed mainly to the different particle size of these samples. For LMP-NR, LMP-VR and LMP-SR, the reduced particle size facilities charger transfer and Li ions diffusion, maximizing the yieldable capacity at high rates.

Fig. 6a compares the cycle stability of the carbon-coated $LiMnPO_4$ samples. The cells were charged to 4.5 V at 0.5 C, kept at 4.5 V for 1 h, and discharged to 2.0 V at 0.5 C. Among the four samples, LMP-VR shows the best cycling stability. After 100 cycles at 0.5 C, LMP-VR can keep a

high discharge capacity 0f 133.5 mAh g^{-1}, corresponding to a retention rate of 87.9%, while LMP-CR can only keep 71.0% of its initial capacity after 100 cycles. Other two plate-like samples, LMP-NR (81.5%) and LMP-SR (80.5%) also exhibit better capacity retention than LMP-CR. Besides the rate capability and cycling stability, working voltage is another important parameter of cathodes to meet the high-energy-density requirement for EVs and HEVs. Fig. 6b compares the rate dependence of median voltage (voltage at half value of the discharge capacity) of $LiMnPO_4$. The LMP-VR maintains a median voltage of over 4 V below 1 C, higher than those of others. The high working voltage at high rates should be ascribed to the enhanced Li ions diffusion kinetics in $LiMnPO_4$ with reduced particle size.

EIS tests were performed to reveal the kinetics parameters in electrode reaction. Prior to the impedance measurements, the cells were charged to the plateau voltage (around 4.17 V) at C/20 and stayed at open circuit voltage for 10 h. As seen in Fig. 7, all the impedance plots consist of a depressed semicircle at the high-to-medium frequency region and a slopping line at the low frequency region. Actually, the depressed semicircle is composed of two partially overlapped semicircles. The first semicircle is related to Li ions transport through the solid surface film, the second one is related to the charge transfer reactions, and the slopping line corresponds to the Li ions diffusion in the bulk material.[24] The plots are fitted by the equivalent circuit given in the inset of Fig. 7, where R_e represents electrolyte resistance, R_f and Q_1 represent surface film resistance and the relax capacitance, R_{ct} and Q_2 denote the charge transfer resistance and the double layer capacitance, and Z_w is the bulk diffusion resistance. According to the fitting results, R_{ct} values of LMP-CR, LMP-NR, LMP-VR and LMP-SR are 71.9, 25.9, 20.3 and 32.6 Ω, respectively. The EIS results agree well with the electrochemical performance of the four $LiMnPO_4$ samples. Obviously,

LMP-VR shows the lowest R_{ct} value due mainly to its smallest particle size. The larger specific surface area and smaller particle size of LMP-VR than those of LMP-CR, LMP-NR and LMP-SR, provide a higher electrolyte contact and shorter Li ions diffusion distance, which lowers the charge transfer resistance and facilitates the electrode reaction and mass transport, leading to the excellent electrochemical performance.

CV scanning was performed to further explain the different electrochemical behaviors of the samples. The cells were charged and discharged at the rate of C/20 for three cycles prior to the CV scanning. Fig. 8 shows the CV plots of the carbon-coated $LiMnPO_4$ samples at various scan rates from 0.05 to 0.5 mV s^{-1}. The cathodic peak currents are equal to the corresponding anodic peak currents for each plot, indicative of good reversibility of all the samples. As seen in Fig. 8e, the peak current is proportional to the square root of the scan rate, confirming that the electrode reaction is a reversible process.[35] For a reversible reaction, the peak currents during anodic scans at different rates could be used to calculate the Li ions chemical diffusion coefficient using the Randles Sevcik equation[35]:

$$\frac{i_p}{m} = 0.4463 n^{3/2} F^{3/2} C^* A_e R^{-1/2} T^{-1/2} D^{1/2} \nu^{1/2} \quad (4)$$

where i_p is the peak currents (A) at different scan rates, m is the mass of electrode, n is charge transfer number, F is the Faraday constant (96485 C mol^{-1}), C is the initial concentration of Li ions in $LiMnPO_4$ (0.0223 mol cm^{-3}), A_e is the effective area (cm^2) that corresponds to the (010) planes (calculated based on particle dimension and BET specific surface area), v is the scan rate (V s^{-1}), R is the gas constant (8.314 J mol^{-1} K^{-1}), T is the absolute temperature (298 K), and D is the diffusion constant (cm^2 s^{-1}). According to the slopes of the fitting lines in Fig. 8e, the Li ions chemical diffusion coefficients of LMP-CR, LMP-NR, LMP-VR and LMP-SR are calculated to be 2.3×10^{-16}, 6.8×10^{-16}, 9.5×10^{-16} and 3.5×10^{-16} cm^2 s^{-1}, respectively. Again, the LMP-VR showed the largest Li

ions diffusion rate, endowing it with best electrochemical performance. The reported *D* values varies from ~10^{-12} to ~10^{-16} cm^2s^{-1} based on the different calculation methods, test modes etc.[22, 24, 36, 37] Considering the one-dimension Li ions diffusion path in $LiMnPO_4$ lattice, better crystallinity, less defects, small size and more exposed (010) faces are very beneficial to increase the *D* values and electrochemical properties.[3, 5]

The results discussed above reveal that high-performance $LiMnPO_4$ cathode can be easily prepared by an EG-based solvothermal process. It is worth noticing that most of the high-performance $LiMnPO_4$ reported previously was tested by charging at a low current (0.1 C or 0.05 C) followed by discharging at high rates. Our study demonstrates that the large discharge capacity can also be realized even the cells are charged also at a large current, which is of great practical application value. We have succeeded in the reuse of the retrieved EG in the synthesis of $LiMnPO_4$. In addition, doubling the starting materials has little effect on the morphology and size of the product (Supporting Information, Fig. S1). Both methods can reduce the cost for $LiMnPO_4$ synthesis. Table 2 compares the preparation methods and electrochemical properties between our work and the best work reported to date. In comparison to other work, we think that this simple, one-plot and additive-free solvothermal method sheds a light on the synthesis of high-performance $LiMnPO_4$ cathode.

Table 2. Comparison of synthesis methods and electrochemical properties of $LiMnPO_4$ materials.

Synthesis approach	Charge current	Specific discharge capacity (mAh g^{-1})	Reference
One-step solvothermal preparation Post carbon coating	Equal to the discharge current	122.5 at 5 C 108.2 at 10 C	This work
Ultrasonic spray pyrolysis Post heat treatment Ball milling with carbon	Charged at C/20	106.7 at 2 C 60 at 10 C	[6]
A complex PMMA template assisted method	Charged at C/10	105 at 10 C	[8]
Liquid-phase exfoliation Solvothermal lithiation	–	119 at 5 C 95 at 10 C	[9]

Conclusions

In summary, we synthesized nanoscaled $LiMnPO_4$ by a facile EG-based solvothermal method. The morphology, particle size and crystal orientation of $LiMnPO_4$ nanocrystals are sensitive to the relative ratio of the three reagents, LiOH, H_3PO_4 and $MnSO_4$. A systematic study has been conducted to understand the significant influence of different ratios of the starting materials and we confirm the critical role of H^+ during the solvothermal process. When using the commonly adopted $LiOH/H_3PO_4/MnSO_4$ ratio of 3:1:1, $LiMnPO_4$ shows a spindle-like shape, which exposes dominant (010) face. By decreasing the amount of LiOH, increasing the proportion of H_3PO_4 or introducing a small amount of H_2SO_4, much smaller-sized plate-like $LiMnPO_4$ with orientation along the (100) face was produced. After carbon coating, all the plate-like $LiMnPO_4$ samples exhibit better rate performance and cycling stability than spindle-like one. Among them, due to the lowest charge transfer resistance and highest Li ion diffusion coefficient，the sample obtained from the $LiOH/H_3PO_4/MnSO_4$ ratio of 3:1.1:1 shows the best electrochemical performance, delivering discharge capacities of 157.4, 143.8, 136.5, 122.5, and 108.2 mAh g^{-1} at 0.1, 1, 2, 5 and 10 C, respectively, which is far superior to those prepared by a similar hydrothermal/solvothermal method previously. This simple, one-spot solvothermal preparation method provide a new method to the synthesis of high-performance $LiMnPO_4$ cathode material.

Acknowledgements

This work was supported by National Basic Research Program of China (2013CB934001), the National Natural Science Foundation of China (No. 51101139), Key Science and Technology Innovation Team of Zhejiang Province under Grant Number 2010R50013, and Program for Innovative Research Team in University of Ministry of Education of China (IRT13037).

References

1 A. K. Padhi, K. Nanjundaswamy and J. B. d. Goodenough, *J. Electrochem.Soc*, 1997, **144**, 1188-1194.

2 D. Choi, J. Xiao, Y. J. Choi, J. S. Hardy, M. Vijayakumar, M. Bhuvaneswari, J. Liu, W. Xu, W. Wang and Z. Yang, *Energy Environ. Sci.*, 2011, **4**, 4560-4566.

3 L.-X. Yuan, Z.-H. Wang, W.-X. Zhang, X.-L. Hu, J.-T. Chen, Y.-H. Huang and J. B. Goodenough, *Energy Environ. Sci.*, 2011, **4**, 269-284.

4 N. S. Choi, Z. Chen, S. A. Freunberger, X. Ji, Y. K. Sun, K. Amine, G. Yushin, L. F. Nazar, J. Cho and P. G. Bruce, *Angew. Chem. Int. Ed.*, 2012, **51**, 9994-10024.

5 V. Aravindan, J. Gnanaraj, Y.-S. Lee and S. Madhavi, *J. Mater. Chem. A*, 2013, **1**, 3518-3539.

6 S. M. Oh, S. W. Oh, C. S. Yoon, B. Scrosati, K. Amine and Y. K. Sun, *Adv. Funct. Mater.*, 2010, **20**, 3260-3265.

7 S. Martha, B. Markovsky, J. Grinblat, Y. Gofer, O. Haik, E. Zinigrad, D. Aurbach, T. Drezen, D. Wang and G. Deghenghi, *J. Electrochem. Soc.*, 2009, **156**, A541-A552.

8 H. Yoo, M. Jo, B. S. Jin, H. S. Kim and J. Cho, *Adv. Energy Mater.*, 2011, **1**, 347-351.

9 X. Rui, X. Zhao, Z. Lu, H. Tan, D. Sim, H. H. Hng, R. Yazami, T. M. Lim and Q. Yan, *ACS nano*, 2013, **7**, 5637-5646.

10 M. K. Devaraju and I. Honma, *Adv. Energy Mater.*, 2012, **2**, 284-297.

11 M.-M. Titirici, M. Antonietti and A. Thomas, *Chem. Mater.*, 2006, **18**, 3808-3812.

12 A. A. Peterson, F. Vogel, R. P. Lachance, M. Fröling, M. J. Antal Jr and J. W. Tester, *Energy Environ. Sci.*, 2008, **1**, 32-65.

13 B. Hu, K. Wang, L. Wu, S. H. Yu, M. Antonietti and M. M. Titirici, *Adv. Mater.*, 2010, **22**, 813-828.

14 W. Shi, S. Song and H. Zhang, *Chem. Soc. Rev.*, 2013, **42**, 5714-5743.

15 S. Yang, P. Y. Zavalij and M. Stanley Whittingham, *Electrochem. Commun.*, 2001, **3**, 505-508.

16 C. Delacourt, P. Poizot, M. Morcrette, J.-M. Tarascon and C. Masquelier, *Chem. Mater.*, 2004, **16**, 93-99.

17 D. Wang, H. Buqa, M. Crouzet, G. Deghenghi, T. Drezen, I. Exnar, N.-H. Kwon, J. H. Miners, L. Poletto and M. Grätzel, J *J. Power Sources*, 2009, **189**, 624-628.

18 T.-H. Kim, H.-S. Park, M.-H. Lee, S.-Y. Lee and H.-K. Song, *J. Power Sources*, 2012, **210**, 1-6.

19 Z. Qin, X. Zhou, Y. Xia, C. Tang and Z. Liu, *J. Mater. Chem.*, 2012, **22**, 21144-21153.

20 S.-L. Yang, R.-G. Ma, M.-J. Hu, L.-J. Xi, Z.-G. Lu and C. Chung, *J. Mater. Chem.*, 2012, **22**, 25402-25408.

21 Y. Cao, J. Duan, G. Hu, F. Jiang, Z. Peng, K. Du and H. Guo, *Electrochim. Acta*, 2013, **98**, 183-189.

22 H.-C. Dinh, S.-i. Mho, Y. Kang and I.-H. Yeo, *J. Power Sources*, 2013, **244**, 189-195.

23 X.-L. Pan, C.-Y. Xu, D. Hong, H.-T. Fang and L. Zhen, *Electrochim. Acta*, 2013, **87**, 303-308.

24 F. Zhou, P. Zhu, X. Fu, R. Chen, R. Sun and C.-p. Wong, *CrystEngComm*, 2014, **16**, 766-774.

25 C. Nan, J. Lu, C. Chen, Q. Peng and Y. Li, *J. Mater. Chem.*, 2011, **21**, 9994-9996.

26 C. Nan, J. Lu, L. Li, L. Li, Q. Peng and Y. Li, *Nano Res.*, 2013, **6**, 469-477.

27 R. Srinivasan, B. Chavillon, C. Doussier-Brochard, L. Cario, M. Paris, E. Gautron, P. Deniard, F. Odobel and S. Jobic, *J. Mater. Chem.*, 2008, **18**, 5647-5653.

28 X. Qin, J. Wang, J. Xie, F. Li, L. Wen and X. Wang, *Phys. Chem. Chem. Phys.*, 2012, **14**, 2669-2677.

29 L. Wang, X. He, W. Sun, J. Wang, Y. Li and S. Fan, *Nano lett.*, 2012, **12**, 5632-5636.

30 K. Dokko, S. Koizumi, H. Nakano and K. Kanamura, *J. Mater. Chem.*, 2007, **17**, 4803-4810.

31 X. Qin, X. Wang, H. Xiang, J. Xie, J. Li and Y. Zhou, *J. Phys. Chem. C*, 2010, **114**, 16806-16812.

32 S. H. Im, Y. T. Lee, B. Wiley and Y. Xia, *Angew. Chem. Int. Ed.*, 2005, **117**, 2192-2195.

33 C. Li, Z. Quan, P. Yang, J. Yang, H. Lian and J. Lin, *J. Mater. Chem.*, 2008, **18**, 1353-1361.

34 L. Qian, J. Zai, Z. Chen, J. Zhu, Y. Yuan and X. Qian, *CrystEngComm*, 2010, **12**, 199-206.

35 Y. Denis, C. Fietzek, W. Weydanz, K. Donoue, T. Inoue, H. Kurokawa and S. Fujitani, *J. Electrochem. Soc.*, 2007, **154**, A253-A257.

36 V. Ramar and P. Balaya, *Phys. Chem. Chem. Phys.*, 2013, **15**, 17240-17249.

37 L. Zhang, Q. Qu, L. Zhang, J. Li and H. Zheng, *J. Mater. Chem. A*, 2014, **2**, 711-719.

Figure captions

Fig. 1 XRD patterns of (a) LMP-CR and (b) LMP-NR.

Fig. 2 SEM images of (a) LMP-CR and (b) LMP-NR.

Fig. 3 TEM images (left and middle-top), HRTEM image (right-top), FFT patterns (middle-bottom) and schematic diagram (right-bottom) of (a) LMP-CR and (b) LMP-NR. The inset in TEM image shows the thickness of the nanoplates.

Fig.4 SEM image, TEM image and FFT patterns of $LiMnPO_4$ nanoparticles: (a) LMP-VR and (b) LMP-SR. The insets in TEM image show the thickness of the nanoplates.

Fig. 5 Voltage profiles of (a) LMP-CR, (b) LMP-NR, (c) LMP-VR and (d) LMP-SR. The cells were charged to 4.5 V at 0.05–10 C, kept at 4.5 V for 1 h, and then discharged to 2 V at the same rate as the charge process.

Fig. 6 (a) Discharge capacity vs. cycle number and (b) median voltage (voltage at half value of the discharge capacity) vs. C rate of LMP-CR, LMP-NR, LMP-VR and LMP-SR. In (a) the cells were charged to 4.5 V at 0.5 C, kept at 4.5 V for 1 h, and then discharged to 2.0 V at 0.5 C.

Fig. 7 Impedance plots of LMP-CR, LMP-NR, LMP-VR and LMP-SR and the corresponding fitting using equivalent circuit (inset).

Fig. 8 CV plots of (a) LMP-CR, (b) LMP-NR, (c) LMP-VR and (d) LMP-SR at different scan rates, and (e) the plots of anodic peak current density (I_p) as a function of the square root of the scan rate ($v^{1/2}$).

Figures

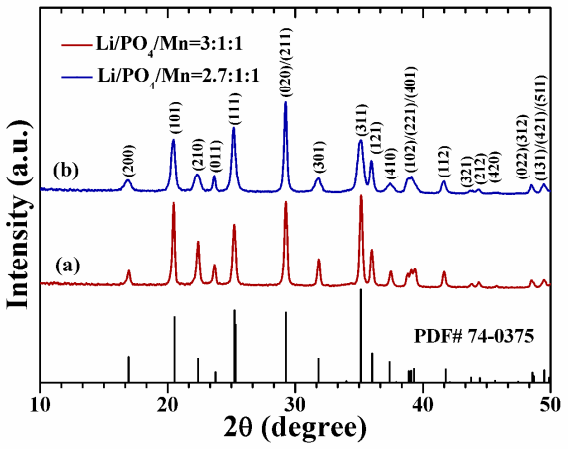

Fig. 1

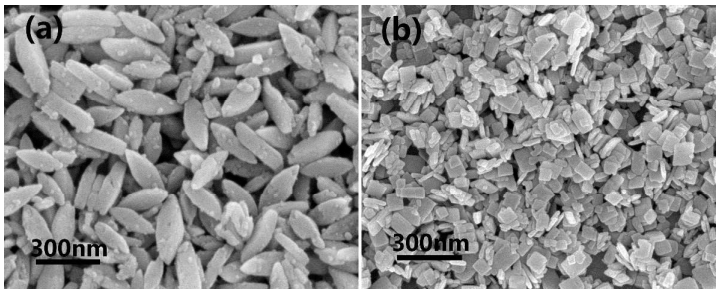

Fig. 2

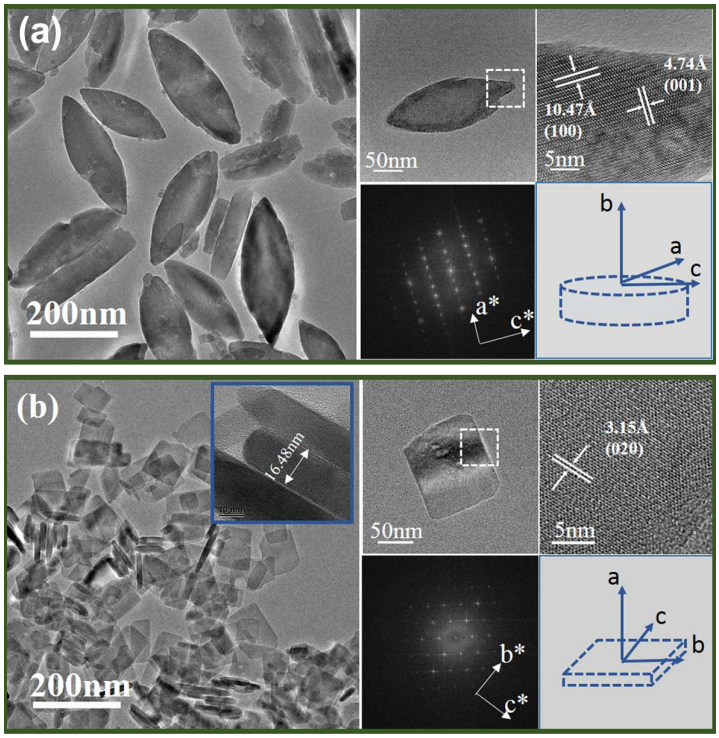

Fig. 3

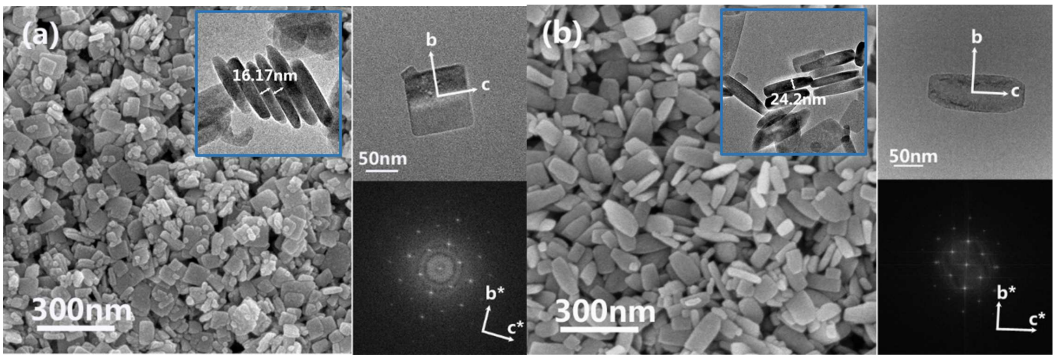

Fig. 4

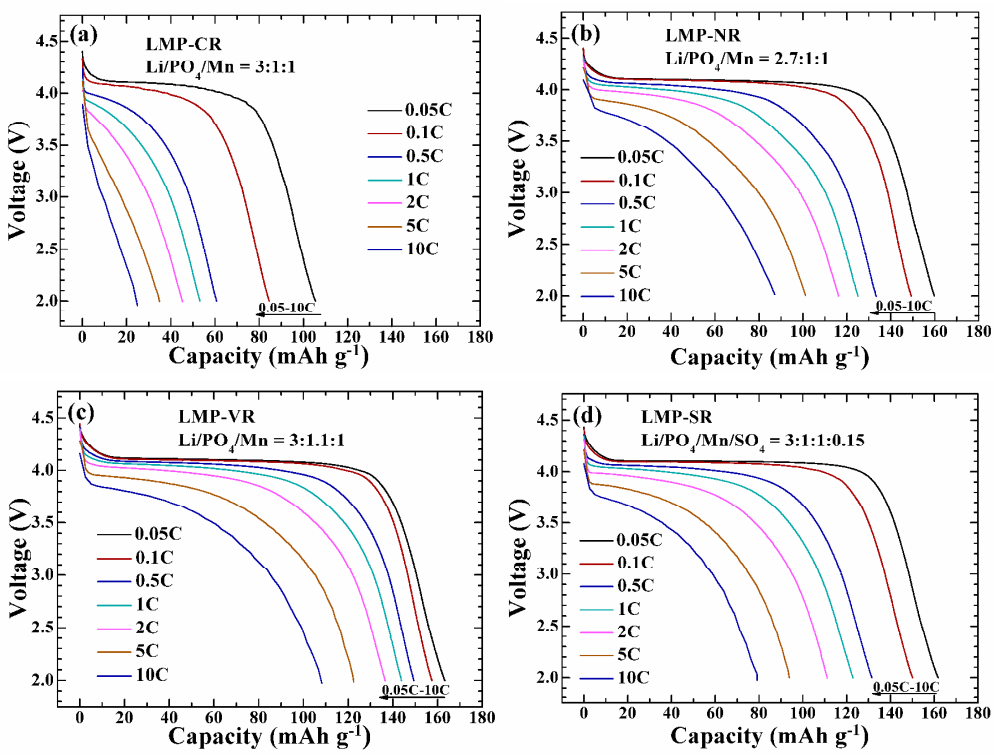

Fig. 5

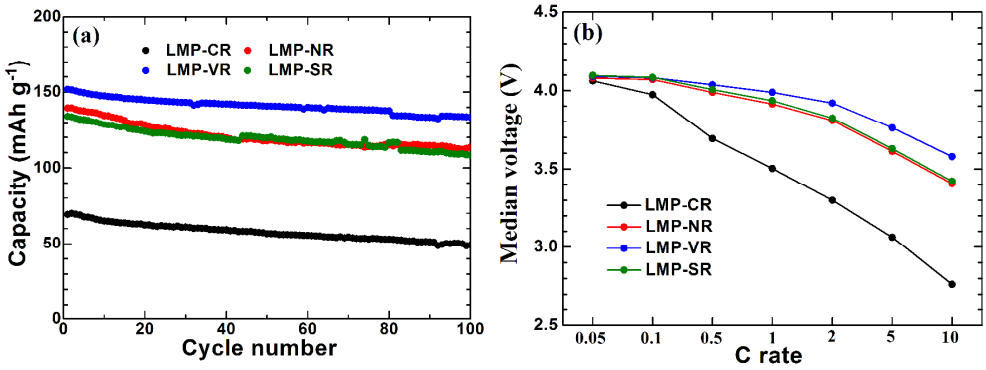

Fig. 6

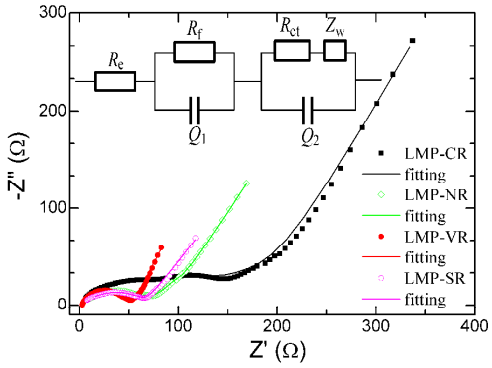

Fig. 7

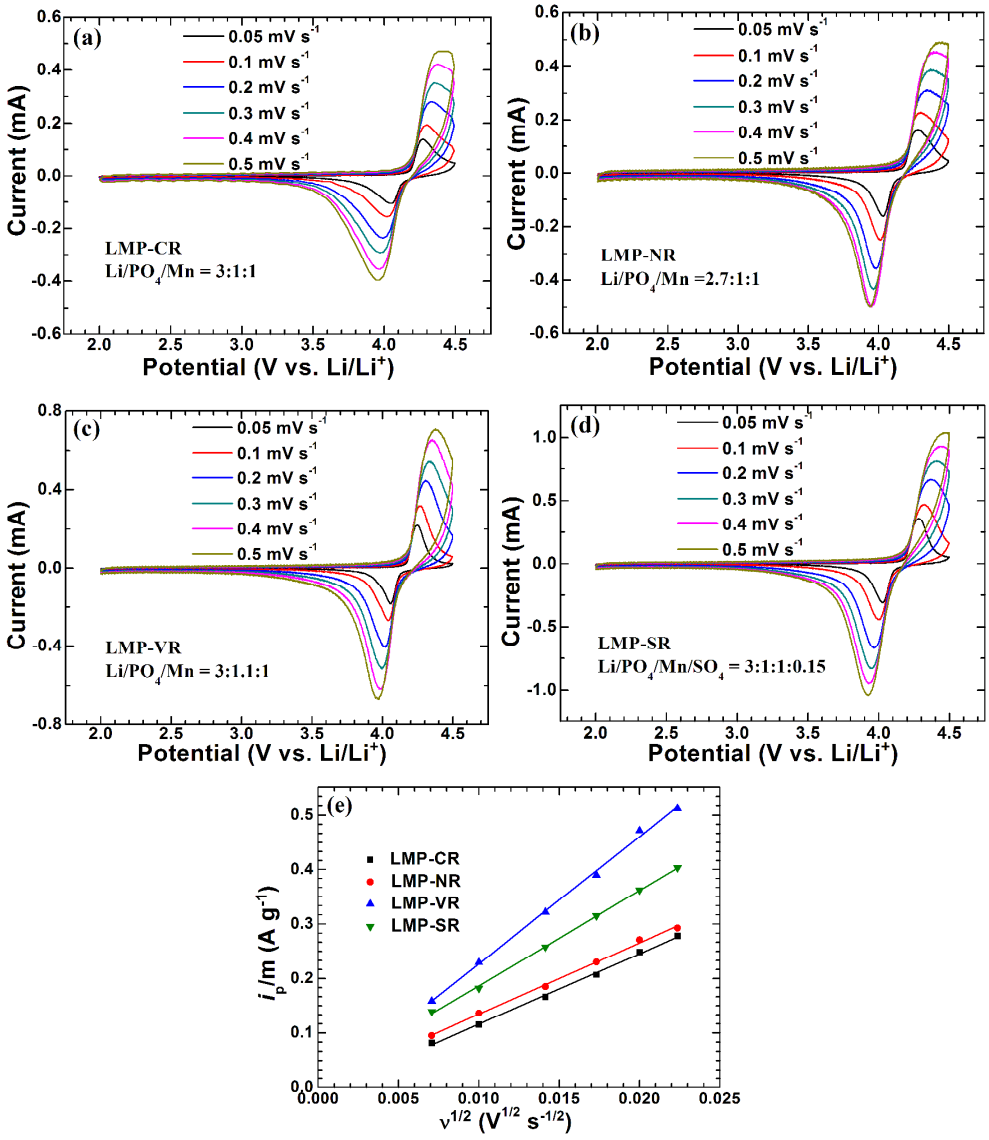

Fig. 8

Table of contents

$LiMnPO_4$ nano-plates exhibit excellent electrochemical performance, delivering a capacity of 108.2 mAh g^{-1} at 10 C and a capacity of 133.5 mAh g^{-1} after 100 cycles at 0.5 C.